ACCOUNTS
of chemical research

One-Dimensional Self-Assembly of Planar π-Conjugated Molecules: Adaptable Building Blocks for Organic Nanodevices

LING ZANG*,†,§, YANKE CHE†,§, AND JEFFREY S. MOORE*,‡
†Department of Chemistry and Biochemistry, Southern Illinois University, Carbondale, Illinois 62901, ‡Departments of Chemistry and Materials Science and Engineering, University of Illinois at Urbana−Champaign, Urbana, Illinois 61801

RECEIVED ON JANUARY 31, 2008

CONSPECTUS

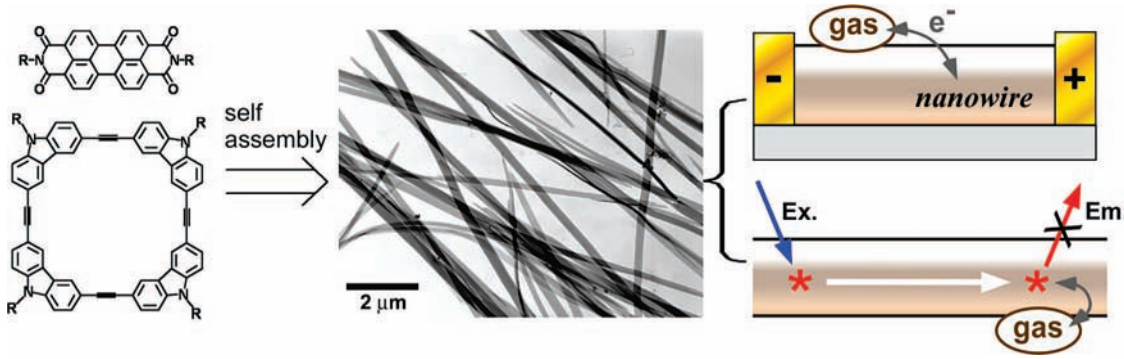

In general, fabrication of well-defined organic nanowires or nanobelts with controllable size and morphology is not as advanced as for their inorganic counterparts. Whereas inorganic nanowires are widely exploited in optoelectronic nanodevices, there remains considerable untapped potential in the one-dimensional (1D) organic materials. This Account describes our recent progress and discoveries in the field of 1D self-assembly of planar π-conjugated molecules and their application in various nanodevices including the optical and electrical sensors. The Account is aimed at providing new insights into how to combine elements of molecular design and engineering with materials fabrication to achieve properties and functions that are desirable for nanoscale optoelectronic applications. The goal of our research program is to advance the knowledge and develop a deeper understanding in the frontier area of 1D organic nanomaterials, for which several basic questions will be addressed: (1) How can one control and optimize the molecular arrangement by modifying the molecular structure? (2) What processing factors affect self-assembly and the final morphology of the fabricated nanomaterials; how can these factors be controlled to achieve the desired 1D nanomaterials, for example, nanowires or nanobelts? (3) How do the optoelectronic properties (e.g., emission, exciton migration, and charge transport) of the assembled materials depend on the molecular arrangement and the intermolecular interactions? (4) How can the inherent optoelectronic properties of the nanomaterials be correlated with applications in sensing, switching, and other types of optoelectronic devices?

The results presented demonstrate the feasibility of controlling the morphology and molecular organization of 1D organic nanomaterials. Two types of molecules have been employed to explore the 1D self-assembly and the application in optoelectronic sensing: one is perylene tetracarboxylic diimide (PTCDI, n-type) and the other is arylene ethynylene macrocycle (AEM, p-type). The materials described in this project are uniquely multifunctional, combining the properties of nanoporosity, efficient exciton migration and charge transport, and strong interfacial interaction with the guest (target) molecules. We see this combination as enabling a range of important technological applications that demand tightly coupled interaction between matter, photons, and charge. Such applications may include optical sensing, electrical sensing, and polarized emission. Particularly, the well-defined nanowires fabricated in this study represent unique systems for investigating the dimensional confinement of the optoelectronic properties of organic semiconductors, such as linearly polarized emission, dimensionally confined exciton migration, and optimal π-electronic coupling (favorable for charge transport). Combination of these properties will make the 1D self-assembly ideal for many orientation-sensitive applications, such as polarized light-emitting diodes and flat panel displays.

Published on the Web 07/11/2008 www.pubs.acs.org/acr
10.1021/ar800030w CCC: $40.75

1. Introduction

Nanostructured, one-dimensional (1D) morphologies (such as nanowires) composed of electronically active constituents have gained increasing interest in the emerging fields of nanoscience and nanotechnology in recent years,[1,2] mainly due to their promising applications in electronic and optoelectronic nanodevices, for which the device miniaturization requires small channel materials. However, most 1D nanostructures reported to date are based on inorganic materials. The analogous research has been much less thoroughly studied on organic materials, while they have already been widely used in thin film based devices such as field-effect transistors, light-emitting diodes, and photovoltaic cells. Organic semiconductors provide many advantages over the inorganic counterparts, such as unlimited choices of molecular structures for property optimization, high flexibility and low cost of materials fabrication, ease for large area processing and compatibility with flexible and lightweight plastic substrates, and thus may open broader applications for the next generation of electronic devices.

Previous evidence from the columnar stacking of discotic liquid crystal molecules has suggested that self-assembly through strong $\pi-\pi$ stacking could be an effective approach to 1D nanostructures for planar, rigid organic molecules.[3−11] This is particularly true for the larger macrocyclic aromatic molecules like hexabenzocoronene.[3] However, it still remains a difficult task to fabricate nanowires or other types of 1D nanostructures with *well-defined morphology and molecular arrangement*. The main difficulty lies in the fact that a successful 1D fabrication demands a tight correlation between the self-assembling kinetics or thermodynamics and the molecular design and engineering, which in turn usually requires a strong interplay between chemical synthesis, materials fabrication and physical characterization, in search of optimal crystalline structure and optoelectronic properties that relate to broad range of applications in nanodevices.

In this Account, we describe our recent progress in control and optimization of the 1D self-assembly of planar π-conjugated macromolecules, which cover both n-type and p-type semiconductor materials and thus are suitable for application in integrated optoelectronic nanodevices. The aim of the Account is not only to demonstrate the increasing importance and emerging research in 1D nanomaterials of organic semiconductors, but moreover to provide new insights into how to combine elements of molecular design and engineering with the materials fabrication to achieve properties and functions that are desirable for nanoscale optoelectronic applications, such as electrical and optical sensing.

2. Molecular Design, Synthesis, and Engineering

The building block molecules employed in the 1D self-assembly described in this Account include two types of molecules: perylene tetracarboxylic diimides (PTCDIs) and arylene ethynylene macrocycles (AEMs). The former forms a class of n-type semiconductor,[12−14] while the latter is of p-type character. Studying both types of semiconductors may provide well-rounded, integrated understanding of the optoelectronic properties of the organic materials and the potential applications in devices utilizing nanostructured materials, which usually require both p- and n-type components. The strong $\pi-\pi$ interaction between the planar aromatic skeletons and their noncollapsible structure make PTCDIs and AEMs ideal candidates for 1D self-assembly. Particularly, PTCDIs form an extremely robust class of molecules with high thermal and photostability. This property, along with the unique n-type character (compared with the more common p-type counterparts in organic semiconductors), makes PTCDIs one type of the most widely used organic materials in various electronic and optoelectronic devices.[14−16] AEMs represent another class of interesting building-block molecules for self-assembly into 1D tubular nanomaterials.[17,18] These molecules consist of a shape-persistent scaffold with a planar conformation, with minimal ring strain and highly tunable ring sizes (0.5−5 nm).

The synthesis of PTCDI is straightforward as shown in Figure 1. The starting material, perylene tetracarboxylic dianhydride (PTCDA), is commercially available in high purity. The relatively higher reactivity of the monoanhydrides brings a great number of options for constructing a wide variety of molecular structures,[16,19] particularly the asymmetric PTCDIs, which are well-suited for cooperative self-assembly into ultralong nanofibril structures as described below. The synthesis of PTCDIs takes advantages of the fact that the two nitrogen positions at the imides of PTCDI are nodes in the π-orbital wave function,[16,19] leading to enormous options for modifying the structures of the two side chains (but without significant altering of the electronic properties and geometry of the PTCDI skeleton). Modification of side chains strongly affects the conformation and strength of molecular stacking of PTCDI molecules when assembled into crystalline materials.[16,19,20] This provides many options for optimizing the molecular structure to achieve shape-defined 1D self-assembly with desired opto-

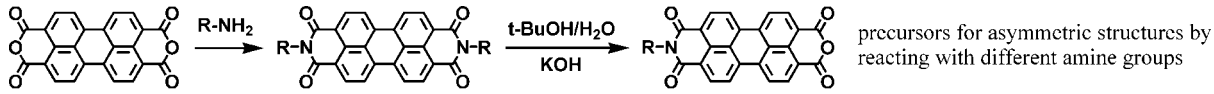

R = side-chains with minimal steric hindrance and maximal enhancement for π–π stacking.

FIGURE 1. General synthesis of PTCDIs and the monoanhydrides.

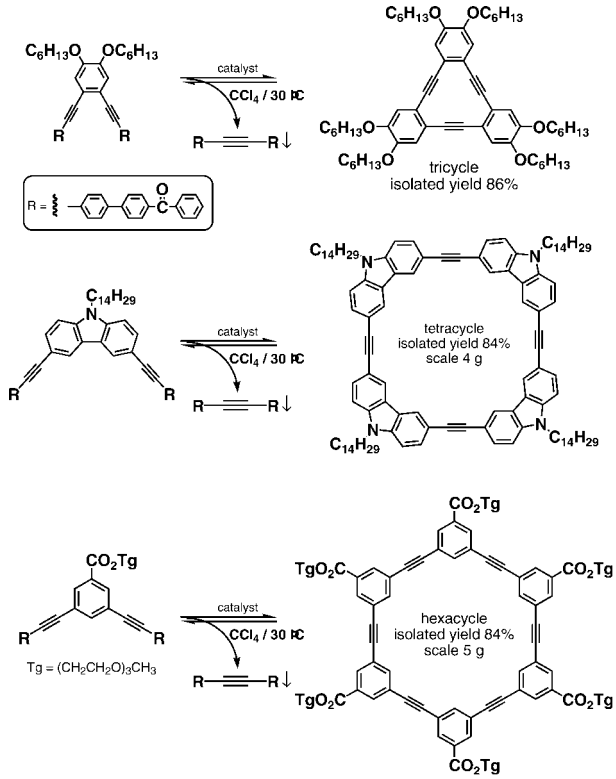

FIGURE 2. Representative examples of precipitation-driven cyclooligomerization of simple precursors leading to high yields of AEMs on the multigram scale.

electronic properties well-suited for various device applications.

A major breakthrough in the synthesis of AEMs came in 2004 when Moore demonstrated that multigram quantities of shape-persistent AEMs can be produced in one step from simple precursors (Figure 2).[21] The approach relies on reversible alkyne metathesis to generate predominately a single cyclooligomeric product. Key developments leading to this breakthrough were the preparation of functional-group tolerant yet highly active alkyne metathesis catalysts and the use of an insoluble byproduct to drive the cyclooligomerization process. As can be seen in Figure 2, the process is general for a variety of functionalized AEMs having a range of sizes and shapes. The straightforward synthesis and highly adaptable modification of cavity size and shape are additional advantages for fabricating AEMs into 1D nanomaterials with tunable optoelectronic properties. The internal void dimensions of these toroidal building blocks can be adjusted by changing the ring size and shape to accommodate various guests or infiltrates (e.g., for molecule-specific sensing).

A general rule for side-chain design is to minimize steric hindrance in order to promote molecular stacking. To this end, linearly configured side chains are usually employed for 1D self-assembly, while the large, bulky, branched side chains like nonyldecyl usually possess strong steric hindrance, restricting extended 1D stacking. Indeed, only irregular chunky aggregates can be formed from the PTCDI molecules modified with nonyldecyl groups, whereas the molecules modified with linear alkyl chains (despite the similar length) can be fabricated into well-defined 1D nanobelt structures under the same self-assembling conditions (Figure 3).[20] Strikingly, such a difference in morphology was observed for both the solution- and surface-based processing. These investigations demonstrate the feasibility of controlling the dimensionality of self-assembly of PTCDI molecules through appropriate side-chain modification in line with proper assembly processing that matches the best the thermodynamics of the molecular structure.

The vital role played by the side chains in the dimensionally controlled self-assembly has also been evidenced in the nanofibril fabrication of AEMs.[22] As shown in Figure 4, introduction of a carbonyl linkage enforces coplanar arrangement between the alkyl side chains and the central skeleton of a tetracyclic AEM. The coplanar geometry enhances the cofacial $\pi-\pi$ stacking, potentially with minimal lateral offset of the molecular stacking, leading more effectively to 1D self-assembly. Indeed, as detailed below, uniform nanofibers can be fabricated from the coplanar tetracycle simply by dispersing (injecting) a molecularly dissolved solution into a poor solvent, or even directly on a surface via vaporization. This is in sharp contrast to the case of the saddle-shaped tetracycle, for which nanofibers can only be formed under strictly controlled assembling conditions, such as gelation from slowly cooled solutions.[22]

3. Solution-Based Self-Assembly

The spontaneous self-assembly of molecules into 1D structures represents a thermodynamic process, where the cofacial $\pi-\pi$ stacking between the molecular skeletons must predominant over the lateral association caused by the hydro-

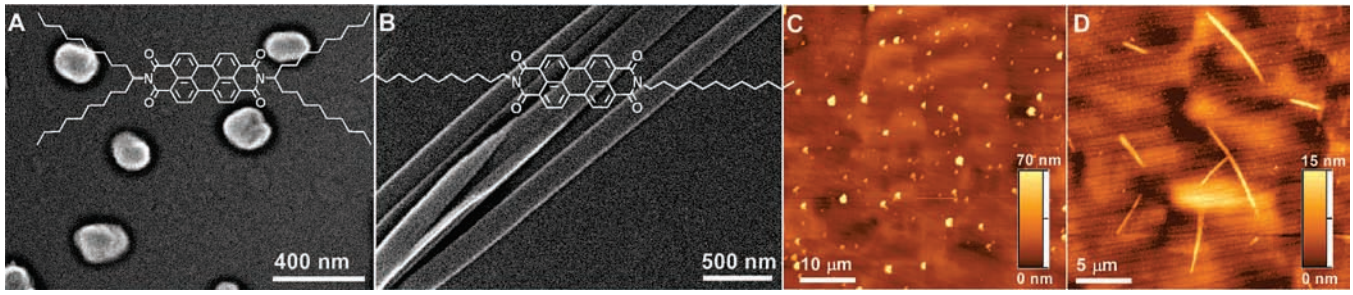

FIGURE 3. Side-chain effect on the self-assembly of PTCDI: (A, B) SEM images taken on the samples fabricated in solutions via phase transfer; (C, D) AFM images taken on the samples fabricated in situ on a glass surface via vapor annealing.

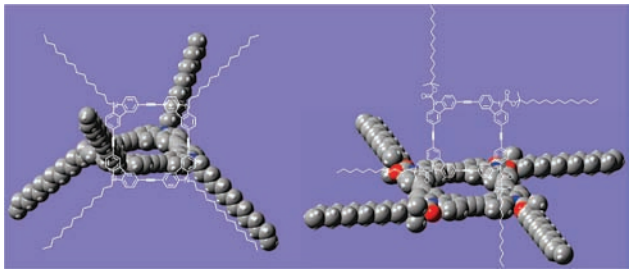

FIGURE 4. Molecular structure and side-chain conformations of two tetracyclic AEMs. A carbonyl linkage promotes coplanar arrangement of the side chains and core skeleton. Energy minimization was achieved by DFT calculation (B3LYP/6-31g*) using Gaussian 03.[32]

phobic interaction among the side chains. The latter usually forces the formation of bulky materials, rather than molecular arrangement along the stacking axis. Developing a 1D self-assembly methodology indeed relies on optimizing the solution processing so as to maximize the longitudinal $\pi-\pi$ stacking against the lateral association. Depending on the molecular structure and geometry (planar vs nonplanar, short vs long side chains, etc.), the self-assembly could be performed via a fast process simply by rapid dispersion of molecules into a "poor" solvent or via a very slow and carefully controlled process like gelation to allow extensive organization of the side chains in a way to maximize the 1D arrangement of the molecular backbones. Described below are several typical protocols that have proven effective in fabrication of well-defined nanowires and nanobelts from both PTCDIs and AEMs.[20,22–29]

Rapid Solution Dispersion. Molecules with predominant $\pi-\pi$ stacking over the lateral side-chain association enables expedient self-assembly of the 1D materials simply by rapid dispersion of the molecules from a "good" solvent into a "poor" solvent (Figure 5),[23] where the molecule has limited solubility and thus self-assembly of the molecules is expected to occur instantaneously. For the PTCDI modified with short linear side chains like propoxyethyl, well-defined nanobelts can simply be obtained by injection of a minimum volume of concentrated chloroform solution of the molecule into a poor solvent like methanol with sufficient stirring of the solution (Figure 5). As monitored by the absorption spectra, the absorption bands of the molecule decreased gradually with time following the injection, while a new band corresponding to the crystal phase appeared at longer wavelengths. The isosbestic point at 536 nm implies a stoichiometric conversion from free molecules to the crystalline phase. Electron diffraction of the nanobelt showed a typical crystalline pattern with sharp diffraction spots (inset of Figure 5C). Two distinct reciprocal lattice vectors can be obtained from the diffraction pattern, giving two *d*-spacings, $d_1 = 0.865$ nm and $d_2 = 0.466$ nm. The d_1 is perpendicular to the belt direction. A similar orientation of the molecular arrangement (with molecule plane approximately perpendicular to the $\pi-\pi$ stacking direction) was also observed by X-ray diffraction for the nanobelts fabricated from other PTCDIs.[20,30]

Phase Transfer. For some molecules, the crystallization (precipitation) proceeds too fast when dispersed into a "poor" solvent from a "good" solvent. This is particularly true when the association (e.g., hydrophobic interaction or hydrogen bonding) between the side chains becomes too strong. In such a case, self-assembling through the simple dispersion protocol (as described above) normally produces large agglomerates. To slow the crystallization process, a so-called phase transfer method as shown in Figure 6 has recently been developed for fabricating discrete fibril structures from these "sticky" molecules, where the slow crystallization is performed at the interface between a "good" and a "poor" solvent.[20] The "poor" solvent (e.g., methanol, hexane) is normally quite distinct (in terms of polarity and density) from the "good" solvent (e.g., chloroform), thus providing the possibility to keep the two solvents in two phases for an extended period.

With the phase transfer methodology, we have successfully fabricated well-defined, discrete nanobelt structures from a PTCDI molecule with long alkyl side chains (Figure 6), which usually allow strong hydrophobic association. In contrast, with the simple dispersion method as described in the last section,

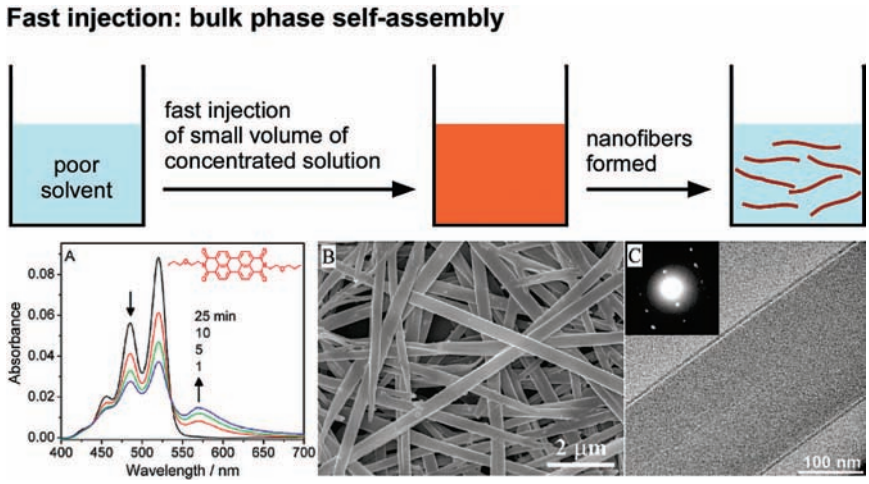

FIGURE 5. Top panel, a scheme showing the self-assembly process via rapid dispersion; bottom panel, (A) absorption spectra showing the formation of crystalline phase (nanobelts) of propoxyethyl-PTCDI when dispersed in methanol, (B) SEM image of the nanobelts (gold stained) cast on glass, and (C) TEM image of a single nanobelt cast on SiO_2 film. Inset shows electron diffraction over a nanobelt cast on carbon film.

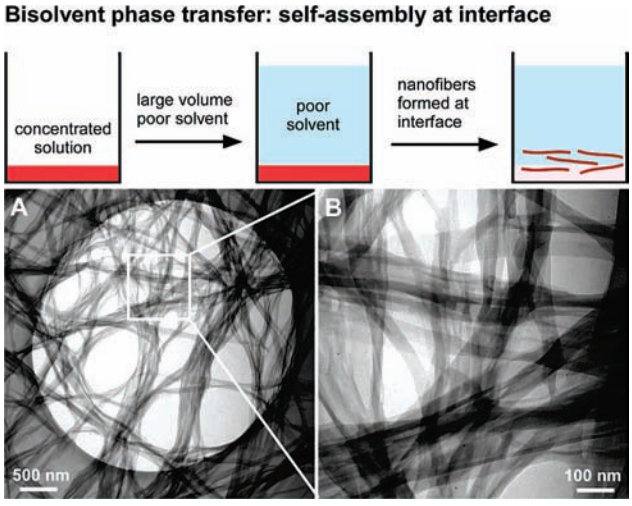

FIGURE 6. Top panel, a scheme showing the self-assembly process via bisolvent phase transfer; bottom panel, (A) TEM images showing the nanobelts of dodecyl-PTCDI lying across a hole of the holey carbon film and (B) a zoomed-in image of panel A.

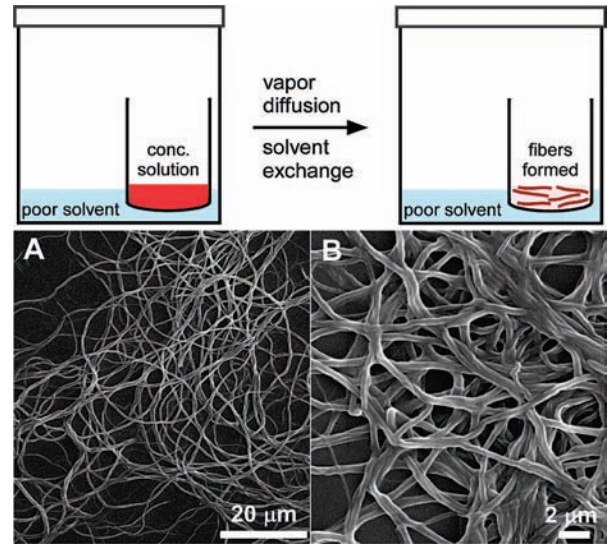

FIGURE 7. Top panel, a scheme showing the self-assembly process via vapor diffusion; bottom panel, (A) SEM image of a nanofibril film deposited on a glass slide and (B) zoom-in SEM image of the nanofibril film.

the same molecule produced highly intertwined fibril piles (which are difficult to disperse as discrete fibrils), likely due to the solvophobically favorable hydrophobic interaction between the side chains. One advantage of the phase transfer method as described in Figure 6 is that it provides a wide range of options for optimizing the assembling process to accommodate molecules with different side-chain structures and sizes. For example, by selection of different solvents, the polarity of the mixed phase at the bisolvent interface can be adjusted over a wide range, providing variability for adjusting the solubility (or crystallization kinetics) for the target molecules and thus allowing for optimization of the self-assembling process.

Vapor Diffusion. The slow crystallization induced by phase transfer at a bisolvent interface as described above can be adapted into an even slower, but more controlled process, via vapor diffusion between two solvents (Figure 7).[28] The slow solvent exchange between the two solvents via vapor diffusion enables gradual, highly controlled adjustment of the solubility of the molecules. The slow decrease in solubility allows for growth of materials with minimal crystalline defects. Moreover, for the molecules with branched side chains, which usually possess significant steric hindrance and thus form ill-defined aggregates when assembled into solid state in a fast way, the slow decrease in solubility may provide the molecules with sufficient time for arranging the side chains in a way favorable for the 1D stacking of the molecules. The other advantage people can take of the vapor diffusion processing

is that the speed of the solvent exchange (or decrease in solubility) can be adjusted by changing the chamber temperature, which in turn changes the vapor pressure of the solvents.

Figure 7 shows the SEM image of the nanofibers fabricated from a half-hydrolyzed PTCDI molecule through a vapor-diffusion process performed in a closed chamber.[28] The average diameter of the nanofibers is ca. 350 nm as determined by zoom-in SEM imaging as shown in Figure 7. The extended 1D molecular arrangement obtained for the molecule is likely dominated by the $\pi-\pi$ interaction between the perylene backbones (which is sterically favored by the bare end of the molecule), in cooperation with the hydrophobic interactions between the side chains of appropriate size.

Seeded Growth. Taking advantages from the slow crystallization process as mentioned above, a seeded self-assembling method was recently developed in our laboratory to fabricate ultralong (millimeter) nanobelts from an asymmetric PTCDI molecule as shown Figure 8.[27] The polyoxyethylene side-chain attachment makes the molecule highly soluble in hydrophilic solvents like ethanol. Taking advantage of the miscibility between alcohol and water, the solubility (or self-assembly) of the molecule can feasibly be controlled by adjusting the volume ratio of water-to-alcohol. Upon increase of the water component, the increase in solvent polarity will force solvophobic association between the alkyl side chains, in a manner similar to the 1D self-assembly of surfactants and other amphiphilic molecules. Such hydrophobic interdigitation will bring the molecules in proximity where the $\pi-\pi$ interaction dominates the molecular packing configuration. The $\pi-\pi$ molecular stacking is likely facilitated by the extended conformation of the polyoxyethylene side chain, which is favored in hydrophilic solvent. Indeed, an ultralong nanobelt structure was obtained from the self-assembly of compound **1** in water/ethanol solution at an appropriate volume ratio, ca. 1:1. As demonstrated by the large-area SEM imaging shown in Figure 8, ultralong fibril structure was formed through a slow 1D crystalline growing process, typically over five days, in a 1:1 water/ethanol solvent. Such a slow crystallization process allows for more organized molecular stacking and more extended growth along the fibril long axis. Most of the fibers are more than 0.3 mm in length, and some of them even reach ca. 0.5 mm. The extended 1D self-assembly is likely dominated by the strong $\pi-\pi$ interaction between the PTCDI scaffolds, as indicated by the X-ray diffraction, for which the typical $\pi-\pi$ stacking peak (with *d*-spacing 3.6 Å) was observed. The *millimeter* long nanobelts thus fabricated will enable more expedient construction of integrated nanoelectronic devices, for which deposition of a wire across multiple parallel electrodes is usually demanded.

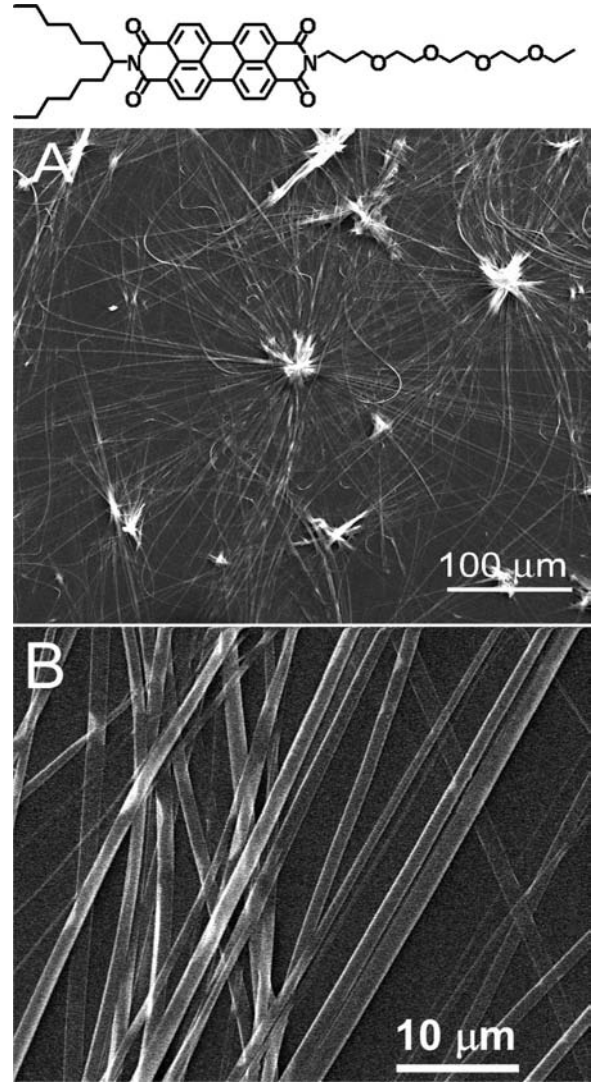

FIGURE 8. (A) A large area SEM image showing the growth of long nanobelts from the central seeding particulate aggregates; (B) a zoom-in image showing the belt morphology and uniform size of the nanobelts.

Sol–Gel Processing. The main challenge in assembling large aromatic molecules into 1D materials lies in balancing the molecular assembly for growth along the π-stacking direction against the lateral association of side chains. This is particularly true for AEM molecules, which normally possess multiple side chains as shown in Figure 2. For these molecules, a simple self-assembling method like rapid dispersion or phase transfer as mentioned above usually produces ill-defined agglomerates, rather than extended 1D structures.

Sol–gel processing is usually an effective way to fabricate well-defined nanofibril structures from molecules modified with multiple long alkyl side chains. Gelation of the molecules is typically realized by cooling a hot, homogeneous solution

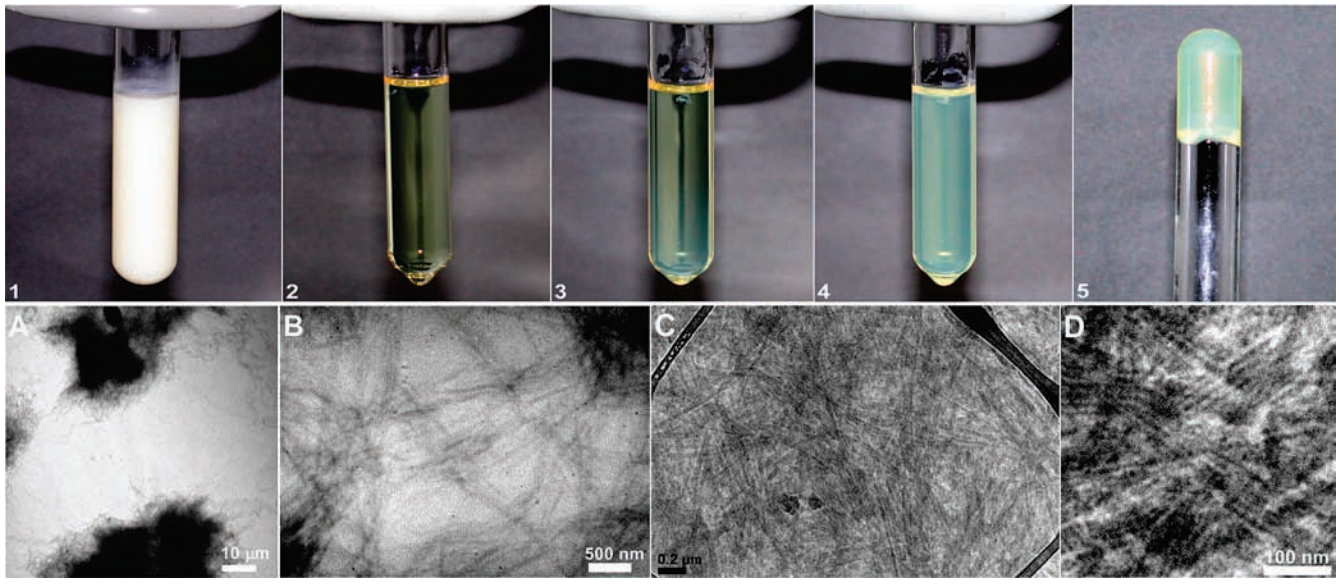

FIGURE 9. Top panel, different stages of the sol−gel process performed on the saddle-like tetracyclic AEM shown in Figure 4: (1) a milky suspension of the molecule in cyclohexane (4 mg/mL) after sonication, (2) totally dissolved after heating at 100 °C in an oil bath, (3) about 2 min after cooling in air; (4) about 5 min after cooling in air, (5) the gel formed after cooling and aging in air for 1 h. Bottom panel, TEM images of the gel deposited on silicon oxide (A, B) and holey carbon (C, D) films: (A) large-area image showing the fibril piles; (B) different sizes of fibril bundles; (C) highly uniform nanofibrils lying across a hole of the carbon film; (D) a zoomed-in image over the sample of C.

from an elevated temperature to room temperature. Such a gelation process decreases gradually the molecular mobility (dynamics) and thus minimizes the lateral growth of the molecular assembly (which is primarily controlled by the side-chain association). Figure 9 shows a robust gelation method recently developed in our laboratory, which has been proven successful for reproducible fabrication of ultrafine nanofibril structures from a tetracycle AEM.[22] Cooling a warm, homogeneous solution of the molecule in cyclohexane from high temperature to room temperature leads to gelation of the solution. During the gelation the molecules become highly organized, with optimal $\pi-\pi$ stacking in cooperation with the side-chain association. A large-area TEM image (Figure 9A) reveals that the dried gel consists of piles of entangled nanofibrils. The strong $\pi-\pi$ stacking gives the fibril structure sufficient mechanical integrity to be transferred onto different substrates. Compared with the polar substrate of silicon oxide as used in Figure 9A,B, a holey carbon film (nonpolar) was also employed as substrate for TEM imaging of the nanofibrils (Figure 9C,D). This robust, durable character of the nanofibril (which allows for easily handling and deposition onto different solid substrates) will be critical for approaching practical applications of the nanoassembly. In general, when the strength of $\pi-\pi$ stacking and the side-chain interactions are not well matched and thus the self-assembly is difficult to control by simple solution-based processing, gelation might be an alternative for approaching the highly organized molecular packing through slow cooling ("freezing") of molecular mobility.

4. Surface-Supported Self-Assembly

Beyond the solution processing methods described above, we have also developed a series of surface-supported self-assembling methods (via either solvent vapor annealing or direct vaporization) for fabricating 1D nanostructures in situ on substrates (Figure 10).[24] Annealing is usually performed in a closed chamber saturated with an appropriate solvent vapor. Depending on the molecular structure and the surface property, solvents of different polarity or a combination of solvents can be used. Factors that influence solvent choice include (1) solubility in order to allow free individual molecules to be transported with the solvent on the surface and (2) minimal affinity to the surface, thus allowing high mobility on the surface. Chloroform is often a good choice for polar surfaces including glass and mica. For the highly planar, rigid molecules, e.g., the tetracycle AEM (Figure 4, right), which demonstrates totally coplanar geometry between the core skeleton and the side chains, the surface-supported self-assembly can even be processed by direct vaporization of the freshly deposited film. The planar geometry of the molecule enables extended $\pi-\pi$ stacking with limited lateral offset, thus allowing for expedient 1D assembly of the molecules via fast vapor-

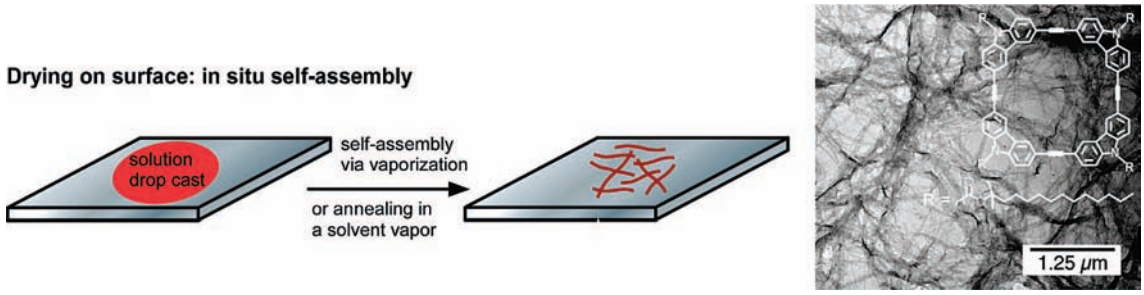

FIGURE 10. A scheme showing the surface-supported self-assembly process via vapor annealing or direct vaporization and a TEM image showing the nanofibrils formed by casting a small amount of THF solution (2 mM) of the coplanar tetracyclic AEM onto a holey carbon film.

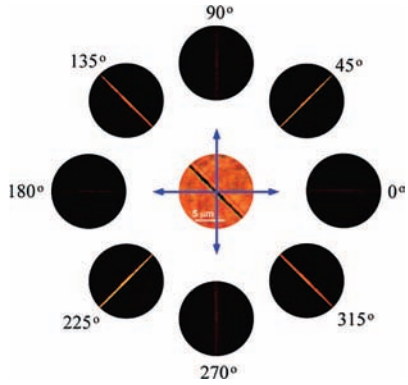

FIGURE 11. A single nanobelt under cross-polarized microscope: consecutive rotation of the sample showed alternate appearance of birefringence as the nanobelt was aligned at 45° to the polarizer. The polarizers are indicated as arrows.

ization. Indeed, uniform nanofibrils were fabricated from the molecule simply by casting a thin film on a substrate, followed by drying in atmosphere. Figure 10 shows a TEM image of the nanofibrils formed on a carbon film. The entangled nanofibrils thus formed on the surface produce a highly porous film that would be ideal for use as a gas sensor potentially with increased sensitivity (vide infra).

5. One-Dimensional Confinement and Enhancement of Exciton Migration: Amplified Fluorescent Sensing

Uniaxial Optical Properties Consistent with 1D Molecular Stacking. One-dimensional self-assembly of planar aromatic molecules (e.g., PTCDI) usually exhibits uniaxial optical properties along the $\pi-\pi$ stacking direction, as observed for the uniaxial columnar packing of discotic liquid crystal molecules. The uniaxial optical property (and the coherent 1D electrical conductivity) may produce a new generation of optical sensors or switches that will potentially yield higher sensitivity. Figure 11 shows the consecutive rotating microscopy imaging of a nanobelt (fabricated from the PTCDI shown in Figure 5) under crossed polarization, where the central image was taken in the bright field. Only when the nanobelt was aligned 45° to the direction of the polarizer was the anisotropy birefringence maximized. At a position parallel to the polarizer, the birefringence of the nanobelt became minimal (hardly detectable). This implies that the optical axis is indeed along the direction of $\pi-\pi$ stacking, which dominates the 1D growth of the nanobelt.

Linearly Polarized Emission Implying 1D Excitonic Confinement. Investigation of the polarized emission at the single-wire level reveals the orientation of molecular arrangement, which determines the transition dipole moment of the molecular assembly. In most cases, the molecular stacking is not perfectly along the long axis of nanowire, leading to a transition dipole moment (polarization) that deviates from the nanowire long axis. Characterization of the linearly polarized emission requires measurement with a single nanowire (to eliminate the interference of the different orientations of multiple nanowires randomly distributed on the surface).

Figure 12 shows the polarized emission measurement recently performed in the Zang's laboratory with the nanobelts self-assembled from propoxyethyl-PTCDI molecules on glass.[25] The measurement was carried out using a near-field scanning optical microscope (NSOM). Placing a planar polarizer before the emission detector changed the emission intensity depending on the polarizer angle with respect to the orientation of the nanobelt. With the polarizer in a position close to perpendicular to the long-axis of the belt, the emission was diminished (Figure 12B), while at a position close to parallel to the nanobelt, the emission was enhanced (Figure 12C). The same polarization was also observed for excitation. Sequentially rotating the emission polarizer (from 0° to 180°) systematically changes the emission intensity in a way depending on the relative angle between the polarizer and the long-axis of the belt, with a minimum of intensity detected at ca. 78°, which is indicative of the tilted molecular stacking along the long axis of the nanobelt (Figure 12D).

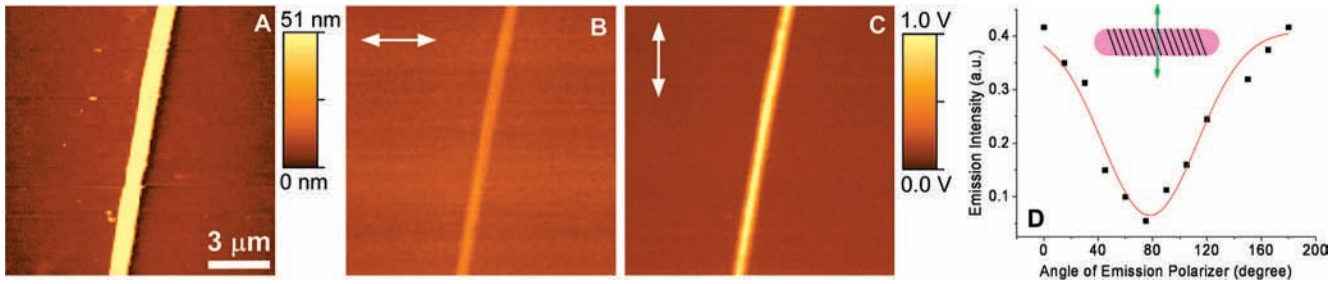

FIGURE 12. (A) NSOM topography image of a nanobelt assembled from propoxyethyl-PTCDI with belt thickness of about 50 nm; (B, C) NSOM emission images collected (by PMT) after a polarizer was placed at horizontal and vertical positions; (D) emission intensity of a single nanobelt depending on the angle between the polarizer and the long axis of the nanobelt. The inset (cartoon) shows the tilted packing of molecules along the long-axis of the nanobelt. The polarizer is indicated as an arrow.

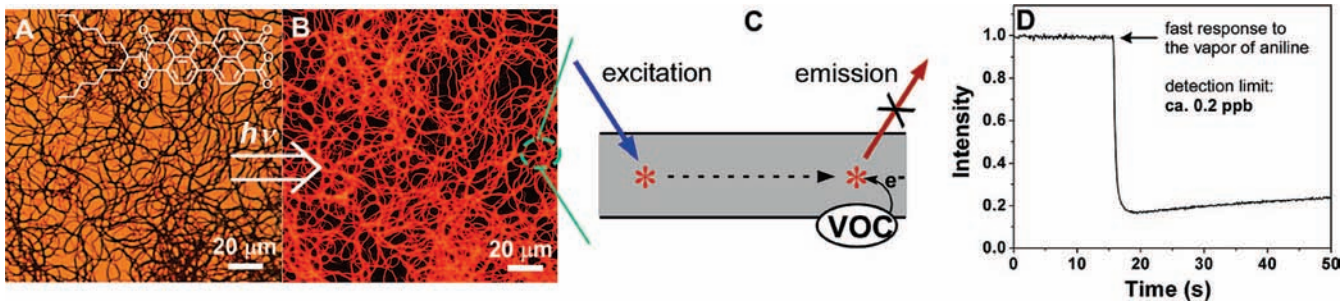

FIGURE 13. (A, B) Bright-field and fluorescence optical microscopy image of a nanofibril film assembled from a half-hydrolyzed PTCDI. Note: due to the diffraction effect the fiber in the optical microscopy image appears larger than the real size as measured by SEM. (C) A schematic diagram showing the mechanism of amplified fluorescence quenching through extended exciton migration along the nanofiber. (D) Time course of fluorescence quenching of the nanofibril film upon blowing with aniline vapor, indicating a response time of only 0.32 s. The fluorescence intensity of the nanofibril film was monitored at $\lambda_{max} = 628$ nm.

Amplified Fluorescence Sensing Based on Nanofibril Films. Consistent with the uniaxial optical properties observed above, the long-range molecular arrangement also leads to *1D enhanced* exciton migration (via intermolecular π-electronic coupling) along the long axis of the nanofiber, enabling amplified fluorescence quenching by the surface adsorbed quencher molecules (Figure 13). Taking advantages of such amplified fluorescence quenching, we have recently fabricated two types of fluorescent sensory materials, which basically consist of nanofibers fabricated from PTCDIs and AEMs. Both types of materials demonstrate efficient fluorescence quenching in response to the adsorption of reducing and oxidizing reagents (particularly the gaseous molecules). When deposited on a substrate, the nanofibers form entangled piles, which produce a mesh-like film that possesses porosity on a number of length scales. Such a porous film not only provides increased surface area for enhanced adsorption of gaseous molecules but also enables expedient diffusion of guest molecules across the film matrix, leading to efficient sensing of the explosives with both high sensitivity and fast time response.

The nanofibers fabricated from the half-hydrolyzed PTCDI (as shown in Figure 7) demonstrate strong fluorescence (with yield ca. 15%) as depicted in the fluorescence microscopy images (Figures 13B), implying a distorted molecular stacking that is usually observed for the PTCDI molecules modified with branched side chains. The molecule possesses a structure that provides a good balance between the molecular stacking and the fluorescence yield of the materials thus assembled. The former prefers a molecular structure with minimal steric hindrance (usually referring to a small or linear side chain), while the latter favors bulky, branched side chains that may distort the π−π stacking to afford increased fluorescence (by enhancing the low-energy excitonic transition) for the molecular assembly.[16,20,23,31] The strong fluorescence of the nanofibers enables development of a fluorescence sensor for detecting reductive volatile organic compounds (VOCs), such as organic amines, through electron-transfer-based fluorescence quenching.[28] Indeed, upon exposure to the saturated vapor of aniline (880 ppm), the fluorescence of the nanofibril film was instantaneously quenched by almost 100%. In comparison, the quenching observed for the nonfibril film fabricated from the symmetric PTCDI molecule modified with two hexylheptyl side chains is only about 5%, apparently due to the poor exciton migration within the less organized film. The efficient fluorescent sensing obtained for the nanofibril film was also observed for a broad range of amines (primary, secondary, and tertiary). The response time for the quenching process (defined as the decay lifetime) was estimated, for

example, at only 0.32 s for the quenching by aniline (Figure 13D). The fast response thus obtained for the nanofibril sensor is consistent with the highly porous structure intrinsic to the mesh-like film, which enables maximal exposure to the amine molecules and expedient diffusion of these molecules throughout the film matrix. The nanofibril sensor also demonstrated high selectivity to organic amines, with minimal response to other common organic reagents. For all the amines tested, more than 85% fluorescence quenching was observed for the nanofibril film upon exposure to the saturated vapor of amines, whereas all the other organic liquids and solids examined as the potential background interference exhibited less than 3% fluorescence quenching under the same testing conditions.[28] Sensitive and selective vapor detection of organic amines is not only critical to air pollution monitoring and control but may also provide expedient methods for food quality control and even medical diagnosis of certain types of disease, for example, uremia and lung cancer, for which biogenic amines released are usually used as the biomarkers. The nanofibril materials, as well as the new sensing module thus developed, may find broad range of applications in health and security examination.

Similar fluorescent sensing of gaseous molecules as described above was also achieved for the nanofibers fabricated from the AEM molecule shown in Figure 10.[29] Compared with the electron-accepting property intrinsic to the PTCDI molecules, the AEM molecule demonstrates strong electron-donating capability, enabling effective sensing of oxidative reagents through electron-transfer-based fluorescence quenching. Oxidative molecules like trinitrotoluene (TNT) and other nitro-based explosives can be detected by these nanofibers at the scale of parts per trillion.[29] Upon deposition onto a suitable substrate, the AEM nanofibers form entangled piles, which in combination with the noncollapsible ring structure of AEMs,[17,18,21] produce a film that possesses porosity on a number of length scales. A porous film consisting of a large number of nanofibers not only provides increased surface area for enhanced adsorption of gaseous molecules but also enables expedient diffusion of guest molecules across the film matrix, leading to efficient sensing, with a signal potentially independent of the film thickness. Combination of these porous properties with the extended exciton migration intrinsic to the individual nanofibers makes the nanofibril film an ideal sensing material for detecting oxidative VOCs like nitro-based explosives (Figure 14).[29] Particularly for TNT, the detection limit was projected as low as 10 ppt (compared with the saturated vapor pressure of 5 ppb), making it possible to detect an explosive resource at a safe remote distance.

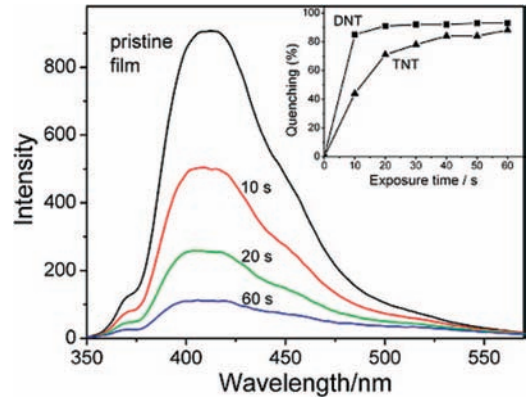

FIGURE 14. Fluorescence spectra of a 90 nm thick nanofibril film fabricated on glass from the coplanar tetracycle AEM (shown in Figure 10) upon exposure to saturated vapor of TNT (5 ppb) at different times. Inset shows a time course of quenching for TNT and DNT.

6. One-Dimensional Enhancement of Charge Transport: Electrical Sensing for Gaseous Reagents

The efficient intermolecular electron transfer between PTCDI and reducing reagents (e.g., hydrazine) leads to the formation of the anionic radical of PTCDI.[26] The radical was so stable in the presence of hydrazine that its UV−vis absorption spectrum could be recorded even under ambient conditions (Figure 15A). More importantly, the charge separation between PTCDI and hydrazine is reversible; that is, the neutral PTCDI can be recovered unchanged by removing the hydrazine via solvent extraction. Steady-state spectral detection of the anionic radical implies the efficient π-delocalization of the charge over the whole PTCDI plane. Such *intramolecular* π-delocalization is conducive to enhancing the charge separation between the stacked molecules within a nanowire. The stable anionic radical was also measured by electron spin resonance (ESR) spectrometry, from which a hyperfine spectrum of the radical was observed (Figure 15B). When stacked together into a columnar phase, the reduced PTCDI does not show hyperfine structure in ESR spectrum. Furthermore, compared with the symmetric spectrum (with **g**-tensor = 2.0033) observed for the free radical (Figure 15C), the ESR spectrum obtained for the nanobelt loses the reflection symmetry about the line center, indicating an anisotropic **g**-tensor, with $g_{\perp}$ (2.0038) > $g_{\parallel}$ (2.0026). The anisotropic **g**-tensor is consistent with the uniaxial property of the nanobelt and implicative of *intermolecular* π-delocalization along the long axis of molecular stacking.

The efficient 1D intermolecular π-delocalization as evidenced above by ESR spectroscopy enables electrical conductivity enhancement of the nanobelt through surface doping of

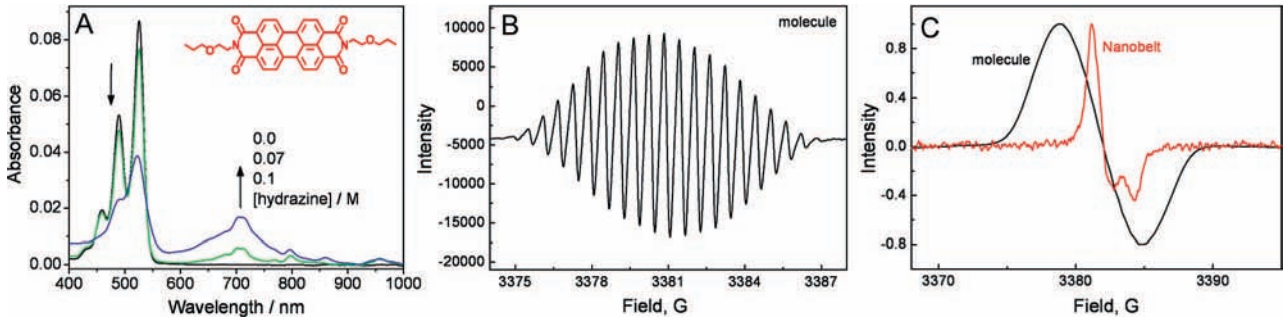

FIGURE 15. (A) UV−vis absorption spectra showing the formation of anionic radical of a PTCDI (1.0 μM in DMF) by electron transfer from hydrazine; (B) hyperfine ESR spectrum of the free anionic radicals of the PTCDI (25 μM in DMSO); (C) comparison of ESR spectra of free anionic radicals dissolved in DMSO (25 μM) and the negatively charged nanobelt dispersed in methanol (1 mM). Intensity was normalized.

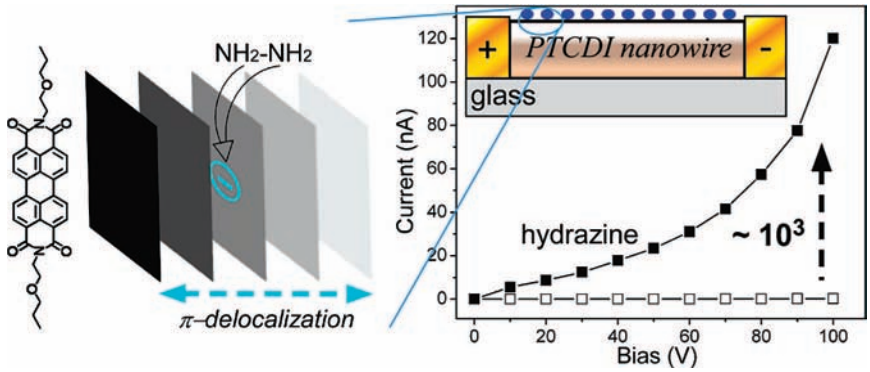

FIGURE 16. Enhancing 1D electrical conductivity (left) through cofacial π-electronic delocalization of doped charges and *I*−*V* curves (right) measured on a single nanobelt fabricated from the PTCDI as shown: (□) in air; (■) in saturated hydrazine vapor. Inset shows a schematic illustration of the two-electrode device fabricated on glass with a single nanofiber deposited across the gap (80 μm).

reducing reagent (or electron donor) as shown in Figure 16,[26,27] where the current−voltage (*I*−*V*) measurement was performed on a single nanobelt fabricated from the same PTCDI molecule shown in Figure 5. The conductivity extracted from the quasi-linear region at low bias (up to 50 V) is ca. 1.0 × 10^{-3} S m^{-1}, a value significantly higher than that measured from many polymer nanowires. The high conductivity observed is consistent with the ordered one-dimensional π−π stacking, which favors the conductivity through cofacial intermolecular π-delocalization. Efficient 1D charge transport will enable fast charge collection at electrodes and meanwhile reduce the charge recombination within the nanowire. When the nanowire was immersed in saturated hydrazine vapor, the electrical current was dramatically increased by about 3 orders of magnitude, mainly due to the electron donation from hydrazine through electron donor−acceptor complexation with PTCDI. Such a charge separation process is facilitated coincidently by the intramolecular π-electron delocalization within the PTCDI skeleton and the intermolecular π-electron delocalization along the long axis of the nanobelt. The high modulation ratio implies potential application of the nanofibers in electrical sensing of a broad range of reducing gaseous species including organic amines.

7. Conclusion and Future Perspective

Molecular building blocks PTCDIs and AEMs possess large, planar, shape-persistent π-surfaces and thus are highly suited for effective π−π stacking and intermolecular electronic delocalization, producing 1D organized materials with efficient exciton diffusion and charge transport. Combination of these features enables efficient optoelectronic sensing with the 1D nanostructured materials, relying on both photonic and electronic modulation in response to surface VOC adsorption (doping). Compared with the conventional thin films employed in organic-based devices, the nanowire provides increased surface exposure to the gaseous phase, leading to enhanced sensing efficiency. To further optimize the optoelectronic properties and improve the sensing efficiency of the nanowires and other 1D molecular assemblies, future research in this field would entail a much tighter collaboration between chemical synthesis, materials fabrication, and physical characterization. Particularly, the 1D self-assembly will be more targeted on those macrocyclic molecules that are highly tunable and adaptable with respect to structure, geometry, size, and redox properties, providing enormous options for optimizing the crystalline structure, internal void dimensions, and electronic

properties of the nanofibers to achieve the maximal sensitivity in optoelectronic sensing. Moreover, the building-block molecules will be designed in a way to allow multiple offsets for the molecular stacking, thus enabling different strengths and modes for π-electronic coupling between molecules. Through combined structural and spectral characterization, the molecular packing will be correlated to the optoelectronic properties of the 1D nanostructures thus fabricated. Such comparative investigations will be crucial for understanding and improving the fundamental processes in organic based nanodevices.

This work was supported by NSF (Grants CMMI 0638571, CAREER CHE 0641353, CHE 0642413 and CBET 730667), ACS-PRF (Grant 45732-G10), and NSFC (Grant 20520120221).

BIOGRAPHICAL INFORMATION

Ling Zang was born in China in 1968, where he received his B.S. in 1991 from Tsinghua University and his Ph.D. in 1995 from the Chinese Academy of Sciences. After about two years stay in Germany as an Alexander von Humboldt Fellow, he moved to the U.S. in 1998 to continue his research, first at Bowling Green State University and then at Columbia University. In 2003, he joined the chemistry faculty at Southern Illinois University, where he was promoted to Associate Professor with tenure in 2008. In the fall of 2008, he moves to University of Utah to join the faculty of the Department of Materials Science and Engineering, where he will be a USTAR associate professor. His current research interest centers on the manipulation of functional nanostructures, nanomaterials and molecular devices, and the characterization at single-molecule and nanometer scales.

Yanke Che was born in China in 1978, where he received his bachelor degree in 2000 from Xi'an Jiaotong University and completed his Ph.D. in 2006 at Institute of Chemistry, Chinese Academy of Sciences. He is currently a research associate in Prof. Ling Zang's group, working on one-dimensional self-assembly of organic molecules and their application in optoelectronics and sensors.

Jeffrey S. Moore was born near Joliet, IL, in 1962. He received his B.S. in chemistry (1984) from the University of Illinois, and his Ph.D. in Materials Science and Engineering with Samuel Stupp (1989). After a NSF position at Caltech with Robert Grubbs, he began his independent career at the University of Michigan in Ann Arbor. He returned in 1993 to the University of Illinois, where he is currently the Murchison-Mallory Professor of Chemistry and Materials Science and Engineering. His research focuses on molecular self-assembly, structure-controlled macromolecules and foldamers, stimuli-responsive materials, and self-healing polymers.

FOOTNOTES

* To whom correspondence should be addressed. E-mail addresses: lzang@eng.utah.edu; jsmoore@uiuc.edu.

§ Present address: Department of Materials Science and Engineering, University of Utah, 122 S. Central Campus Drive, Salt Lake City, UT 84112.

REFERENCES

1 Hu, J.; Odom, T. W.; Lieber, C. M. Chemistry and physics in one dimension: Synthesis and properties of nanowires and nanotubes. *Acc. Chem. Res.* **1999**, *32*, 435–445.

2 Xia, Y.; Yang, P.; Sun, Y.; Wu, Y.; Mayers, B.; Gates, B.; Yin, Y.; Kim, F.; Yan, H. One-dimensional nanostructures: Synthesis, characterization, and applications. *Adv. Mater.* **2003**, *15*, 353–389.

3 Wu, J.; Pisula, W.; Muellen, K. Graphenes as potential material for electronics. *Chem. Rev.* **2007**, *107*, 718–747.

4 Schenning, A. P. H. J.; Meijer, E. W. Supramolecular electronics; nanowires from self-assembled p-conjugated systems. *Chem. Commun.* **2005**, 3245–3258.

5 Nguyen, T.-Q.; Martel, R.; Avouris, P.; Bushey, M. L.; Brus, L.; Nuckolls, C. Molecular interactions in one-dimensional organic nanostructures. *J. Am. Chem. Soc.* **2004**, *126*, 5234–5242.

6 Wang, Z.; Medforth, C. J.; Shelnutt, J. A. Porphyrin nanotubes by ionic self-assembly. *J. Am. Chem. Soc.* **2004**, *126*, 15954–15955.

7 Shirakawa, M.; Fujita, N.; Shinkai, S. A stable single piece of unimolecularly pi-stacked porphyrin aggregate in a thixotropic low molecular weight gel: A one-dimensional molecular template for polydiacetylene wiring up to several tens of micrometers in length. *J. Am. Chem. Soc.* **2005**, *127*, 4164–4165.

8 Hill, J. P.; Jin, W.; Kosaka, A.; Fukushima, T.; Ichihara, H.; Shimomura, T.; Ito, K.; Hashizume, T.; Ishii, N.; Aida, T. Self-assembled hexa-peri-hexabenzocoronene graphitic nanotube. *Science* **2004**, *304*, 1481–1483.

9 Kato, T. Self-assembly of phase-segregates liquid crystal structures. *Science* **2002**, *295*, 2414–2418.

10 van Hameren, R.; Schoen, P.; van Buul, A. M.; Hoogboom, J.; Lazarenko, S. V.; Gerritsen, J. W.; Engelkamp, H.; Christianen, P. C. M.; Heus, H. A.; Maan, J. C.; Rasing, T.; Speller, S.; Rowan, A. E.; Elemans, J. A. A. W.; Nolte, R. J. M. Macroscopic hierarchical surface patterning of porphyrin trimers via self-assembly and dewetting. *Science* **2006**, *314*, 1433–1436.

11 Zhao, Y. S.; Fu, H.; Hu, F.; Peng, A. D.; Yao, J. Multicolor emission from ordered assemblies of organic 1D nanomaterials. *Adv. Mater.* **2007**, *19*, 3554–3558.

12 Xu, B. Q.; Xiao, X.; Yang, X.; Zang, L.; Tao, N. J. Large gate modulation in the current of a room temperature single molecule transistor. *J. Am. Chem. Soc.* **2005**, *127*, 2386–2387.

13 Li, X.; Xu, B. Q.; Xiao, X.; Yang, X.; Zang, L.; Tao, N. J. Controlling charge transport in single molecules using electrochemical gate. *Faraday Discuss.* **2006**, *131*, 111–120.

14 Newman, C. R.; Frisbie, C. D.; da Silva Filho, D. A.; Bredas, J.-L.; Ewbank, P. C.; Mann, K. R. Introduction to organic thin film transistors and design of n-channel organic semiconductors. *Chem. Mater.* **2004**, *16*, 4436–4451.

15 Zang, L.; Liu, R.; Holman, M. W.; Nguyen, K. T.; Adams, D. M. A single-molecule probe based on intramolecular electron transfer. *J. Am. Chem. Soc.* **2002**, *124*, 10640–10641.

16 Wurthner, F. Perylene bisimide dyes as versatile building blocks for functional supramolecular architectures. *Chem. Commun.* **2004**, 1564–79.

17 Zhao, D.; Moore, J. S. Shape-persistent arylene ethynylene macrocycles: Syntheses and supramolecular chemistry. *Chem. Commun.* **2003**, 807–818.

18 Moore, J. S. Shape-persistent molecular architectures of nanoscale dimension. *Acc. Chem. Res.* **1997**, *30*, 402–413.

19 Langhals, H. Cyclic carboxylic imide structures as structure elements of high stability. novel developments in perylene dye chemistry. *Heterocycles* **1995**, *40*, 477–500.

20 Balakrishnan, K.; Datar, A.; Naddo, T.; Huang, J.; Oitker, R.; Yen, M.; Zhao, J.; Zang, L. Effect of side-chain substituents on self-assembly of perylene diimide molecules: Morphology control. *J. Am. Chem. Soc.* **2006**, *128*, 7390–7398.

21 Zhang, W.; Moore, J. S. Shape-persistent macrocycles: Structures and synthetic approaches from arylene and ethynylene building blocks (a review). *Angew. Chem., Int. Ed.* **2006**, *45*, 4416–4439.

22 Balakrishnan, K.; Datar, A.; Zhang, W.; Yang, X.; Naddo, T.; Huang, J.; Zuo, J.; Yen, M.; Moore, J. S.; Zang, L. Nanofibril self-assembly of an arylene ethynylene macrocycle. *J. Am. Chem. Soc.* **2006**, *128*, 6576–6577.

23 Balakrishnan, K.; Datar, A.; Oitker, R.; Chen, H.; Zuo, J.; Zang, L. Nanobelt self-assembly from an organic n-type semiconductor: Propoxyethyl-PTCDI. *J. Am. Chem. Soc.* **2005**, *127*, 10496–10497.

24 Datar, A.; Oitker, R.; Zang, L. Surface-assisted one-dimensional self-assembly of a perylene based semiconductor molecule. *Chem. Commun.* **2006**, 1649–1651.

25 Datar, A.; Balakrishnan, K.; Yang, X. M.; Zuo, X.; Huang, J. L.; Yen, M.; Zhao, J.;

Tiede, D. M.; Zang, L. Linearly polarized emission of an organic semiconductor nanobelt. *J. Phys. Chem. B* **2006**, *110*, 12327–12332.

26 Che, Y.; Datar, A. X. Y.; Naddo, T.; Zhao, J.; Zang, L. Enhancing one-dimensional charge transport through cofacial π-electronic delocalization: Conductivity improvement for organic nanobelts. *J. Am. Chem. Soc.* **2007**, *129*, 6354–6355.

27 Che, Y.; Datar, A.; Balakrishnan, K.; Zang, L. Ultralong nanobelts self-assembled from an asymmetric perylene tetracarboxylic diimide. *J. Am. Chem. Soc.* **2007**, *129*, 7234–7235.

28 Che, Y.; Yang, X.; Loser, S.; Zang, L. Expedient Vapor Sensing of Organic Amines Using Fluorescent Nanofibers Fabricated from an n-Type Organic Semiconductor. *Nano Lett.* **2008**, in press.

29 Naddo, T.; Che, Y.; Zhang, W.; Balakrishnan, K. X. Y.; Yen, M.; Zhao, J.; Moore, J. S.; Zang, L. Sensitive Detection of Explosives with a Fluorescent Nanofibril Film. *J. Am. Chem. Soc.* **2007**, *129*, 6978–6979.

30 Briseno, A. L.; Mannsfeld, S. C. B.; Lu, X.; Xiong, Y.; Jenekhe, S. A.; Bao, Z.; Xia, Y. Fabrication of Field-Effect Transistors from Hexathiapentacene Single-Crystal Nanowires. *Nano Lett.* **2007**, *7*, 668–675.

31 Ahrens, M. J.; Sinks, L. E.; Rybtchinski, B.; Liu, W.; Jones, B. A.; Giaimo, J. M.; Gusev, A. V.; Goshe, A. J.; Tiede, D. M.; Wasielewski, M. R. Self-Assembly of Supramolecular Light-Harvesting Arrays from Covalent Multi-Chromophore Perylene-3,4:9,10-bis(dicarboximide) Building Blocks. *J. Am. Chem. Soc.* **2004**, *126*, 8284–8294.

32 Frisch, M. J.; Trucks, G. W.; Schlegel, H. B.; Scuseria, G. E.; Robb, M. A.; Cheeseman, J. R.; Montgomery, J. A., Jr.; Vreven, T.; Kudin, K. N.; Burant, J. C.; Millam, J. M.; Iyengar, S. S.; Tomasi, J.; Barone, V.; Mennucci, B.; Cossi, M.; Scalmani, G.; Rega, N.; Petersson, G. A.; Nakatsuji, H.; Hada, M.; Ehara, M.; Toyota, K.; Fukuda, R.; Hasegawa, J.; Ishida, M.; Nakajima, T.; Honda, Y.; Kitao, O.; Nakai, H.; Klene, M.; Li, X.; Knox, J. E.; Hratchian, H. P.; Cross, J. B.; Bakken, V.; Adamo, C.; Jaramillo, J.; Gomperts, R.; Stratmann, R. E.; Yazyev, O.; Austin, A. J.; Cammi, R.; Pomelli, C.; Ochterski, J. W.; Ayala, P. Y.; Morokuma, K.; Voth, G. A.; Salvador, P.; Dannenberg, J. J.; Zakrzewski, V. G.; Dapprich, S.; Daniels, A. D.; Strain, M. C.; Farkas, O.; Malick, D. K.; Rabuck, A. D.; Raghavachari, K.; Foresman, J. B.; Ortiz, J. V.; Cui, Q.; Baboul, A. G.; Clifford, S.; Cioslowski, J.; Stefanov, B. B.; Liu, G.; Liashenko, A.; Piskorz, P.; Komaromi, I.; Martin, R. L.; Fox, D. J.; Keith, T.; Al-Laham, M. A.; Peng, C. Y.; Nanayakkara, A.; Challacombe, M.; Gill, P. M. W.; Johnson, B.; Chen, W.; Wong, M. W.; Gonzalez, C.; Pople, J. A. *Gaussian 03*, Revision C.02, Gaussian, Inc.: Wallingford CT, 2004.